SHAPE FLUCTUATIONS AND CRITICAL PHENOMENA

Reinhard Lipowsky

Sektion Physik der Universität München,
Theresienstr. 37, 8000 München 2, FRG

I. INTRODUCTION AND OUTLINE

Low-dimensional objects or manifolds such as interfaces, vortices or flux lines, membranes, and polymers are usually soft and flexible and, thus, undergo shape fluctuations which lead to a variety of critical phenomena. First of all, a fluctuating manifold represents a scale-invariant state which can be characterized by critical exponents. /1/ Depending on the strength of the fluctuations, this state may be *smooth, rough or crumpled.* In some systems, the manifold can undergo a transition between these different states; e.g., interfaces can undergo *roughening transitions* from smooth to rough states /2/ while (model) membranes can undergo *crumpling transitions* from rough to crumpled states /3/.

Many physical phenomena such as, e.g., wetting, adhesion and adsorption are governed by the mutual interaction of these low-dimensional manifolds. /4/ Quite generally, the shape fluctuations of these objects *renormalize* their direct interaction arising from intermolecular forces. This renormalization acts to increase the repulsive part of the interaction. In fact, sufficiently strong fluctuations overcome the attractive part of the direct interaction and lead to phase transitions from bound to unbound states of the manifolds. For interfaces, membranes, and polymers, these *unbinding transitions* represent wetting, adhesion, and adsorption transitions, respectively.

This paper is organized as follows. First, Sec. II contains a brief introduction to the physics of shape fluctuations. In Sec. III, the scale-invariance of rough and crumpled states, and the critical behavior at roughening and crumpling transitions is reviewed. In Sec. IV, a nontrivial example is described in some detail: the roughening of interfaces in quasiperiodic systems. Finally, the interplay of direct and fluctuation-induced interactions and the associated unbinding transitions are discussed in Sec. V.

II. SHAPE FLUCTUATIONS.

A. Fluctuations of interfaces and flux lines governed by tension.

An *interface* or domain wall represents the contact region between two bulk phases of matter. /5/ Its macroscopic shape is governed by the interfacial free energy or *tension,* Σ,

which is the work (per unit area) required to create new interfacial area. If the two phases, say α and β, are both fluid, Σ is isotropic, and a macroscopic chunk of β phase surrounded by α phase has a spherical shape (in the absence of gravity). On the other hand, if one of the two phases is crystalline, the tension Σ is anisotropic and leads to the possibility of facets.

On mesoscopic scales, i.e., on scales which are larger than the molecular size but smaller than the size of the α and β domains, the interface does not have a fixed shape but undulates and thus undergoes shape fluctuations which lead to a certain interfacial *roughness*. These fluctuations do *not* conserve the total (intrinsic) area of the manifold and, thus, are governed by the tension Σ. For a liquid-vapor interface, these excitations represent *capillary waves*. For a crystal surface, i.e., for a crystal-vapor interface, the shape fluctuations are built up from microscopic *steps* or *ledges* which separate atomically flat terraces on the surface.

The interfaces described so far have been 2-dim surfaces separating 3-dim bulk domains. Condensed matter physics also provides a variety of 2-dim bulk systems containing 1-dim interfaces. /6/ Examples are domain boundaries (i) in monolayers of small molecules adsorbed onto a crystal surface, or (ii) in monolayers or bilayers of amphiphilic molecules adsorbed onto the air-water interface. Sometimes, these 1-dim domain boundaries form a superlattice such as the striped phase near a commensurate-incommensurate transition.

A vortex or *flux line* within a type-II superconductor represents a thin rod or thread of normal conducting material which contains one or several magnetic flux quanta. /7/ These flux lines start to penetrate the superconductor at a lower critical value of the external magnetic field. Close to this critical field, the lines are well separated and form a more or less ordered array. The undulations of these flux lines are controlled by their *line tension.*

Two different excitation mechanism for the fluctuations of interfaces and flux lines must be distinguished: (i) At finite temperatures, $T > 0$, these manifolds fluctuate in order to increase their configurational *entropy*; and (ii) In the presence of quenched impurities (or frozen randomness), they adapt their shape to the randomness in order to minimize their *energy.* The latter mechanism acts even at $T = 0$

B. Fluctuations of membranes and polymers governed by bending elasticity.

Membranes are ultrathin sheets or plates of molecules. Particularly important examples are monolayers and bilayers which form spontaneously in solutions of amphiphilic molecules. /8/ Monolayers arise, e.g., in microemulsions, i.e. in mixtures of water, oil, and surfactant where they separate water from oil domains. Bilayers are typically formed when lipid molecules are dissolved in water. /9/ These latter membranes represent the universal building block of all biomembranes and, thus, provide the spatial organization of biological systems.

Isolated bilayers in water form closed surfaces or vesicles which often have a linear size $\sim$ 10 μm. The shape of these vesicles has been studied in many experiments. These studies support the theoretical concept that the average shape of membranes is controlled by

bending rigidity. /10/ Likewise, typical shape fluctuations of membranes represent thermally-excited *bending modes*.

The bending rigidity is mainly determined by the internal structure of the membrane. Lipid bilayers, e.g., typically exhibit a *crystalline* (L_β)-phase at low T and a *fluid* (L_α)-phase at high T. In a crystalline membrane, the lipid molecules form a fixed network while they diffuse freely within a fluid membrane. Therefore, crystalline membranes are more rigid than fluid ones. The rigidity can also be increased by polymerization of the lipid molecules which leads to a *tethered* membrane.

For sufficiently rigid membranes, the bending modes give rise to a certain *roughness* and, thus, play a role which is completely analogous to the capillary modes of interfaces. In principle, very soft membranes could become highly convoluted or *crumpled*. Indeed, such a behavior is expected from the standard model for fluid membranes /10/ which leads to a finite *persistence length,* ξ_p, for their normal vectors /11/. However, real membranes do not self-intersect and this acts against crumpling. In fact, recent computer simulations indicate that *tethered* membranes do not crumple at finite T because of their self-avoidance. /12/

Crumpled states are, of course, well established for *polymers,* i.e., for long rodlike molecules. /13/ Such macromolecules are formed by chemical reactions in which a huge number of monomers is linked together. Both artificial polymers and biopolymers often consist of $> 10^5$ monomers. On small scales, they should behave like elastic rods and, thus, should also exhibit thermally-excited bending modes. However, with the possible exception of polyelectrolytes, all polymers are expected to have a finite persistence length, ξ_p, for their tangent vectors. This length is often microscopic, and the polymer then forms a random coil, when viewed on the scale of μm's. In this crumpled state, the polymer behaves like a chain of mass points which are connected by harmonic springs with an *entropically generated* spring constant $\sim$ T.

III. SCALE INVARIANCE OF LOW - DIMENSIONAL MANIFOLDS

A. Rough manifolds.

Now, let us consider a *single* manifold such as an interface, flux line, membrane or polymer embedded in a d–dim system. The system is taken to be in thermal equilibrium at temperature T. Furthermore, let us first assume that the system does not contain any type of frozen randomness. Then, the manifold will attain a completely smooth (or flat) state at zero temperature, T = 0, in order to minimize its energy. At finite T > 0 , on the other hand, the manifold will usually develop bumps or wiggles and thus will acquire a certain roughness in order to increase its configurational entropy. Alternatively, one can introduce some frozen randomness into the system which roughens the manifold even at T = 0

To proceed, let us choose a parametrization for the fluctuations of the manifold from its completely smooth state. First, the space dimensionality, d, is decomposed according to

$$d = d_\parallel + d_\perp \qquad (3.1)$$

where $d_\parallel$ is the intrinsic dimensionality of the manifold. Its fluctuations are then described by a displacement field $\mathbf{z} = (z_1,...,z_{d_\perp})$ with $\mathbf{z} = \mathbf{z}(\mathbf{x})$ and $\mathbf{x} = (x_1,...,x_{d_\parallel})$ The completely smooth state at $T = 0$ corresponds to $\mathbf{z} =$ const. Since all components of $\mathbf{z}$ are taken to be single-valued functions of $\mathbf{x}$, manifold fluctuations with overhangs are not included. This means that *gradients* of the fluctuations, ∇z_α with $\nabla \equiv (\partial/\partial x_1, \; ... \; ,\partial/\partial x_{d_\parallel})$ are implicitly assumed to be *small.*

The shape fluctuations of the manifold can now be characterized by the behavior of the difference correlation function,

$$\Delta C_z(\mathbf{x}) \equiv \tfrac{1}{2} < \left[\mathbf{z}(\mathbf{x}) - \mathbf{z}(0)\right]^2 > \qquad (3.2)$$

In some systems, the function $\Delta C_z(\mathbf{x})$ remains bounded from above for arbitrarily large $\mathbf{x}$. This behavior defines a *smooth state* of the manifold. On the other hand, the difference correlation function $\Delta C_z(\mathbf{x})$, may grow without bounds for large $\mathbf{x}$ corresponding to a *rough state* of the manifold. Such a situation is typically characterized by [14]

$$\Delta C_z \sim x^{2\zeta} \quad \text{for large } x \qquad (3.3)$$

where ζ is the socalled *roughness exponent.* Such a behavior of ΔC_z implies that $\Delta C_z(\mathbf{x}/b) \approx \Delta C_z(\mathbf{x})/b^{2\zeta}$ for $x >> a$ where b is an arbitrary rescaling factor and a the small-scale cutoff. Therefore, the shape fluctuations of a rough manifold are (asymptotically) scale-invariant under the rescaling transformation

$$\mathbf{x} \to \mathbf{x}/b \quad \text{and} \quad \mathbf{z} \to \mathbf{z}/b^\zeta \quad . \qquad (3.4)$$

In order to visualize this scale invariance, choose a manifold segment of linear size, L_{in}, and intrinsic area, $L_{in}^{d_\parallel}$. Then, the linear size, $L_\parallel$, of the projected area, $L_\parallel^{d_\parallel}$, and the typical amplitude, $L_\perp$, of the manifold fluctuations, see Fig. 1(a) below, scale as

$$L_\parallel \sim L_{in} \quad \text{and} \quad L_\perp \sim L_\parallel^\zeta \sim L_{in}^\zeta \quad . \qquad (3.5)$$

For *thermally-excited* fluctuations, a single manifold with roughness exponent ζ can be described by the effective Hamiltonian

$$\mathscr{H}\{\mathbf{z}\} = \int d^{d_\parallel}x \; \tfrac{1}{2} K \sum_{\alpha=1}^{d_\perp} (\nabla^n z_\alpha)^2 = \int \frac{d^{d_\parallel}p}{(2\pi)^{d_\parallel}} \tfrac{1}{2} K \, p^{2n} \sum_{\alpha=1}^{d_\perp} |\tilde{z}_\alpha(p)|^2 \qquad (3.6)$$

with

$$n = \zeta + d_\parallel/2 \qquad (3.7)$$

where K represents an effective tension or bending rigidity.

For the model as given by (3.6), the difference correlation function ΔC_z defined in (3.2) is

$$\Delta C_z(x) = d_\perp \, (T/K) \int \frac{d^{d\|}p}{(2\pi)^{d\|}} \, [1 - \exp(i\mathbf{p}\cdot\mathbf{x})]/p^{2n}. \tag{3.8}$$

where a high-momentum cutoff $\sim 1/a$ is implicitly contained. For $d_\| > 2n$, the difference correlation function as given by (3.8) is bounded for large x and the manifold is *smooth*. For $d_\| = 2n$, one has a marginally rough manifold with $\Delta C_z(x) \sim ln(x/a)$ for large x. Finally, for $2n > d_\| > 2-2n$, (3.8) leads to a *rough* manifold characterized by

$$\Delta C_z(x) \approx d_\perp(T/K) \, c_\infty \, x^{2\zeta} \quad \text{with} \quad \zeta = n - d_\|/2 \tag{3.9}$$

for large x where the coefficient c_∞ depends on $d_\|$ but is independent of the cutoff, a.

For an interface with $d = d_\|+1$ the roughness exponent ζ depends on d (or $d_\|$) and on the nature of the two phases separated by the interface. /1/ If both phases are fluid, the interfacial fluctuations are governed by the effective Hamiltonian (3.6) with $n = 1$ (and $d_\perp = 1$) which leads to $\zeta = 0(\sqrt{log})$ in $d = 3$ and $\zeta = (3-d)/2$ in $1 < d < 3$, see (3.9).

The same value of ζ applies to an interface which feels a *periodic* lattice potential provided T exceeds the roughening temperature, T_r, see Sec. III.C below. *Quasiperiodic* lattice potentials, on the other hand, can *lower* the value of ζ/15,16/ as will be explained in Sec. IV. If the two phases separated by the interface contain quenched impurities, the roughness exponent ζ is typically *increased* : a random field system is believed to exhibit /17,18/ $\zeta = (5-d)/3$ for $2 < d < 5$ while a random bond system (with short-range correlated randomness) is characterized by /19,20/ $\zeta = 2/3$ in $d = 1+1$.

A flux line in $d = 1+d_\perp$ subjected to thermally-excited fluctuations, is governed by the effective Hamiltonian (3.6) with $n = 1$ and $d_\| = 1$ which implies $\zeta = 1/2$ according to (3.9). /21/ In the presence of quenched impurities (with short-range correlations), the flux line in $d = 1+2$ should exhibit $\zeta \simeq 0.6$. /22/

The roughness of membranes in $d = 2+d_\perp$ depends on their internal structure. *Fluid* membranes with vanishing shear modulus are governed by bending elasticity alone which corresponds to an effective Hamiltonian as in (3.6) with $d_\| = 2$ and $n = 2$ /10/ It then follows from (3.9) that $\zeta = 1$. /23,24/ *Tethered* membranes, on the other hand, are more rigid and have $\zeta < 1$ /25,26/ : for zero and finite bending rigidity, numerical simulations in $d = 3$ gave the estimates /12/ $\zeta \simeq 0.8$ and /27/ $\zeta = 0.63 \pm 0.02$, respectively. Finally, polymers in $d = 1+d_\perp$, when treated as stiff rods governed by bending elasticity, are described by the effective Hamiltonian (3.6) with $d_\| = 1$ and $n = 2$ which implies $\zeta = 3/2$ according to (3.9).

As mentioned, the parametrization in terms of displacement fields, $\mathbf{z}(\mathbf{x})$, assumes that the gradients of $\mathbf{z}$ are small. The overall gradient of a hump as shown in Fig.1(a) is $\sim$

$(L_\perp/L_\parallel) \sim L_{in}^{\zeta-1}$ where L_{in} measures the intrinsic size of the manifold segment. Thus, for $\zeta <$ 1, the overall gradient *decreases* on large scales and the parametrization in terms of z should be adequate. On the other hand, for $\zeta \geq 1$, the overall gradient grows for large L_{in}. In the latter case, overhangs of the manifold fluctuations are essential and the parametrization $z(x)$ is no longer appropriate on large scales.
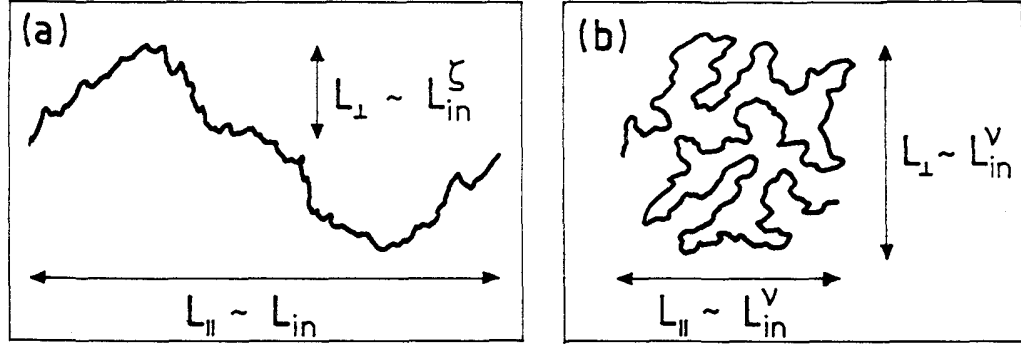
Fig.1:   (a) Typical *hump* of a rough manifold, and (b) typical *blob* of a crumpled manifold with intrinsic size L_{in}. These states are characterized by the roughness exponent ζ and the crumple exponent ν, respectively, see (3.5) and (3.17).

B. Scale invariance of crumpled manifolds.

For roughness exponent $\zeta \geq 1$, the manifold develops many overhangs on sufficiently large scales and, thus, becomes highly convoluted or *crumpled,* see Fig.1(b). If the topology of the $d_\parallel$–dim manifold is not changed by the fluctuations, such a crumpled state can be parametrized by $r = [r,(s),..,r_d(s)]$ with an internal coordinate $s = (s_1,..,s_{d_\parallel})$

For a (linear) polymer chain with $d_\parallel = 1$, one has $r = [r,(s),..,r_d(s)]$ where the coordinate s is taken to be the *arclength.* The thermally-excited bending modes can now be characterized by the more general difference correlation function

$$\Delta C_r(s) \equiv \tfrac{1}{2} < [\, r(s)-r(0)]^2 > \; = \; \tfrac{1}{2} \int_0^s ds_1 \int_0^s ds_2 \; <d\hat{t}/ds_1)\cdot(d\hat{t}/ds_2)> \qquad (3.10)$$

where $\hat{t}(s) \equiv dr/ds$ is the unit tangent vector. This function contains a characteristic *persistence length,* ξ_p, and is expected to exhibit the scaling form

$$\Delta C_r(s) \approx \xi_p^2 \; \mathscr{D}(s/\xi_p) \qquad . \qquad (3.11)$$

For large $s \gg \xi_p$, the polymer is crumpled and the shape function $\mathscr{D}(y)$ behaves as

$$\mathscr{D}(y) \approx c_\infty y^{2\nu} \quad \text{for large } y \gg 1 \tag{3.12}$$

which defines the *crumple exponent* (or Flory exponent or radius of gyration exponent) ν. If the persistence length ξ_p is large compared to microscopic scales, one has a crossover to a rough state of the polymer characterized by

$$\mathscr{D}(y) \approx y^2 - c_0 y^{2\zeta} \quad \text{for } y \ll 1 \quad \text{with } \zeta = 3/2 \ . \tag{3.13}$$

As a simple example consider a self-intersecting polymer in $d = 1+1$ parametrized by $\mathbf{r}(s) = [r_1(s), r_2(s)]$. The thermally-excited bending modes are then governed by

$$\mathscr{H}\{\hat{t}\} = \int ds \ \tfrac{1}{2} K(d\hat{t}/ds)^2 = \int ds \ \tfrac{1}{2} K(d^2\mathbf{r}/ds^2)^2 \tag{3.14}$$

where $d^2\mathbf{r}/ds^2$ is the local *curvature* of the polymer and K represents an effective bending rigidity. For this simple model, the difference correlation function as given by (3.10) can be calculated explicitly. One then finds the persistence length $\xi_p = 2K/T$ and the scaling form (3.11) with

$$\tfrac{1}{2} \mathscr{D}(y) = y - 1 + \exp(-y) \quad . \tag{3.15}$$

For $y \gg 1$, this leads to $D(y) \approx y$ and, thus, to the crumple exponent $\nu = 1/2$. For $y \ll 1$, on the other hand, one recovers (3.13) with $\zeta = 3/2$

The value $\nu = 1/2$ applies, in fact, to linear polymers in general d provided one allows for self-intersections. For *self-avoiding* polymers, ν depends on d and one has $\nu = 3/4$ and $\nu \simeq 3/5$ in $d = 1+1$ and $d = 1+2$, respectively, as obtained from the Flory argument. /13/

The behavior $\Delta C_r(s) \sim s^{2\nu}$ for large s implies that the shape fluctuations of a crumpled polymer are (asymptotically) scale-invariant under the rescaling transformation

$$s \to s/b \quad \text{and} \quad \mathbf{r} \to \mathbf{r}/b^\nu \quad . \tag{3.16}$$

Thus, a polymer segment of intrinsic length $s \simeq L_{in}$ has an extrinsic size $L_\perp \sim L_\parallel$ with

$$L_\perp \sim L_\parallel \sim L_{in}^\nu \tag{3.17}$$

see Fig. 1(b). The scale $L_\perp \sim L_\parallel$ is conveniently measured by the *radius of gyration*. The relation (3.17) is, in fact, quite general. It also applies to *branched* polymers provided L_{in}/a is taken to be the number of momomers within a connected piece of the branched structure.

Crumpled states are also expected for membranes. First, consider a *tethered* membrane, i.e., a fixed network of molecules connected by tethers or springs. /28,3/ The fluctuations of such a membrane are quasi-isometric, i.e., the intrinsic distance between two molecules in the membrane is roughly independent of the membrane configuration. For an ideal (or

phantom) membrane with self-intersections, a segment with intrinsic area $\sim L_{in}^2$ has the size $L_\perp \sim L_\parallel \sim [ln(L_{in}/a)]^{1/2}$ in $d = 2+d_\perp$. /28/ However, self-avoidance represents a very strong constraint. This can be understood if one considers strictly isometric deformations of a plane, which are obtained by folding the membrane in one direction only. The corresponding bending energy is proportional to the bending energy of a self-avoiding polymer in $d = 1+1$ which implies that a membrane segment with intrinsic area $\sim L_{in}^2$ has $L_\perp \sim L_{in}^{3/4}$ and $L_\parallel \sim L_{in}$. This leads to the estimate $\nu \simeq 7/8$ since $(L_\perp L_\parallel)^{1/2} \sim L_{in}^{7/8}$. As mentioned, recent computer simulations indicate, in fact, that self-avoiding tethered membranes have $\nu = 1$ and are *not* crumpled. /12/

For a *fluid* membrane, the molecules can diffuse freely. The shape of these membranes is believed to be governed by curvature energies alone. The standard model of Helfrich /10/ leads to a finite persistence length $\xi_p \simeq a \exp(2\pi K/T)$ where K is the bending rigidity, /11/ The state of a fluid membrane for $L \gg \xi_p$ is not well understood. It is possible that the membrane develops many fingers in order to increase its entropy and becomes a branched polymer. The typical diameter of these fingers should be set by the persistence length, ξ_p Then, a membrane segment of intrinsic area L_{in}^2 can form fingers with an overall length $L_o \sim L_{in}^2/\xi_p$. A self-avoiding branched polymer with L_o/a monomers has a radius of gyration, $L_\perp \sim L_\parallel \sim L_o^\nu$, with /29/ $\nu \simeq 0.5$ in $d = 3$. This implies that the radius of gyration of a crumpled fluid membrane scales as $L_\perp \sim L_\parallel \sim L_{in}^\nu$ with $\nu \simeq 1$ if the membrane indeed behaves as a branched polymer on large scales.

C. Roughening and Crumpling Transitions.

In the last two sections, we encountered smooth, rough, and crumpled states of fluctuating manifolds. These different states can be distinguished by their long-range order (LRO) *within the d–dim* (embedding) *space.*

For a manifold with $d_\parallel = 1$, *orientational* LRO means that its tangent vectors have a preferred direction. Likewise, a manifold with $d_\perp = 1$ is orientationally ordered if its normal vectors point, on average, into a certain direction. One can then choose a straight line ($d_\parallel = 1$) or a planar hypersurface ($d_\perp = 1$), as a reference state which has the same orientation as the fluctuating manifold. *Translational* order or disorder is now defined in terms of the displacements of the manifold from this reference state. A manifold exhibits translational LRO if these displacements are bounded from above on arbitrarily large scales.

By definition, a *smooth* state exhibits both translational and orientational LRO within the d–dim system. A *rough* manifold, on the other hand, is translationally disordered since its displacements from the smooth reference state become arbitrarily large. For roughness exponent $\zeta < 1$, a rough manifold still exhibits orientational LRO. For $\zeta \geq 1$, on the other

hand, the manifold becomes orientationally disordered as soon as the linear scales exceed the persistence length, ξ_p. In the latter case, the manifold is *crumpled.*

In some systems, the low-dim manifolds undergo a *roughening transition* from a *smooth* state at low T to a *rough* state at high T. At the roughening temperature, $T = T_r$, the manifold is rough with a roughness exponent ζ_r which, in general, can differ from ζ for $T > T_r$. As T_r is approached from below, the large-scale configurations of the manifold can be viewed as an ensemble of humps. The largest humps are statistically independent and characterized by a lateral extension, $\xi_\parallel$, and a transverse extension, $\xi_\perp$, see Fig. 2(a). For scales $L_\parallel \ll \xi_\parallel$, the manifold already exhibits the scale-invariance governed by ζ_r and $L_\perp \sim L_\parallel^{\zeta_r}$. Therefore, a large hump, which has an intrinsic size ξ_{in}, is characterized by $\xi_\parallel \sim \xi_{in}$ and $\xi_\perp \sim \xi_{in}^{\zeta_r}$, compare Fig.1(a) and 2(a). For a continuous roughening transition, this implies that the critical exponents ν_{in}, $\nu_\perp$ and $\nu_\parallel$ defined by
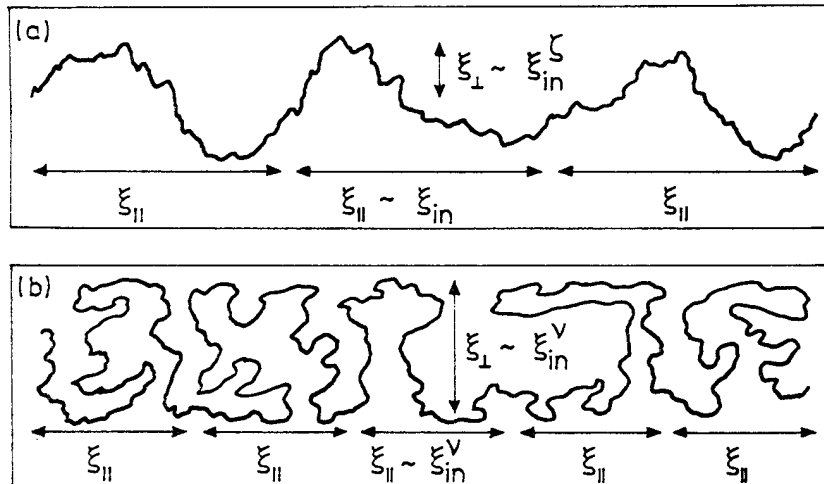
$$\xi_{in} \sim (T_r-T)^{-\nu_{in}}, \quad \xi_\perp \sim (T_r-T)^{-\nu_\perp} \quad \text{and} \quad \xi_\parallel \sim (T_r-T)^{-\nu_\parallel} \tag{3.18}$$

satisfy the scaling relation

$$\nu_\perp = \zeta_r \, \nu_\parallel = \zeta_r \, \nu_{in} \, . \tag{3.19}$$

If the manifold is only marginally rough with $\zeta_r = O(\sqrt{\log})$ at $T = T_r$, one has

$$\xi_\perp \sim [ln(\xi_\parallel/a)]^{1/2} \, . \tag{3.20}$$

Fig.2: (a) Smooth manifold close to a *roughening* transition as an ensemble of humps, and (b) Rough manifold close to a *crumpling* transition as an ensemble of blobs. The length scales, ξ_{in}, $\xi_\perp$, and $\xi_\parallel$ diverge at the transitions, see (3.18) and (3.21)

A roughening transition occurs for an interface in $d = 2+1$ in a *periodic* lattice potential. /2/ In this case, the interface is marginally rough with $\zeta = \zeta_r = 0(\sqrt{\log})$ for $T \geq T_r$ However, $\xi_\parallel \sim \exp(c/\sqrt{T_r-T})$ which implies $\xi_\perp \sim (T_r-T)^{-\nu_\perp}$ with $\nu_\perp = 1/4$ via (3.20).

More recently, roughening transitions have been found for interfaces in $d = 1+1$ arising from *quasiperiodic* lattice potentials. /15,30,31/ In these systems, the roughness exponent ζ_r at $T = T_r$ satisfies $0 < \zeta_r < 1/2$ and, typically, differs from ζ for $T > T_r$. Thus, one has the power-law behavior given by (3.18) and (3.19) as will be explained in Sec. IV below.

Now, consider a manifold which undergoes a *crumpling transition* from a *rough* state at low T to a *crumpled* state at high T. At the crumpling temperature, $T = T_{cr}$, the manifold is crumpled with a crumple exponent ν_{cr} which, in general, will differ from the crumple exponent ν for $T > T_{cr}$. As T_{cr} is approached from below, the manifold configurations can be viewed as an ensemble of *blobs*. The largest blobs with intrinsic size, ξ_{in} can be regarded as statistically independent with extrinsic size $\xi_\perp \sim \xi_\parallel \sim \xi_{in}^{\nu_{cr}}$ within the d–dim system, see Fig. 2(b). If the crumpling transition is continuous, one may define critical exponents ν_{in}, $\nu_\perp$ and $\nu_\parallel$ by

$$\xi_{in} \sim (T_{cr}-T)^{-\nu_{in}} \, , \, \xi_\perp \sim (T_{cr}-T)^{-\nu_\perp} \text{ and } \xi_\parallel \sim (T_{cr}-T)^{-\nu_\parallel} \tag{3.21}$$

in close analogy with (3.18) but now one has the scaling relation

$$\nu_\perp = \nu_\parallel = \nu_{cr} \, \nu_{in} \quad . \tag{3.22}$$

Then, a large manifold segment of intrinsic size $L_{in} \gg \xi_{in}$ has a projected size $L_\parallel \sim (\xi_\parallel/\xi_{in})$ L_{in}. As T_{cr} is approached from below, the prefactor $\xi_\parallel/\xi_{in}$ goes to zero as long as $\xi_\parallel \sim \xi_{in}^{\nu_{cr}}$ with $\nu_{cr} < 1$. Thus, one has

$$L_\parallel \sim (T_{cr} - T)^\beta L_{in} \tag{3.23}$$

with

$$\beta = \nu_{in} (1-\nu_{cr}) \quad . \tag{3.24}$$

Crumpling transitions have been theoretically found for *self-intersecting* manifolds with $d_\parallel > 2$ /32/, and for *self-intersecting* tethered membranes with $d_\parallel = 2$ and finite bending rigidity /25,33-35/. For the latter case, a mean-field theory gives /34/ $\beta = \nu_{cr} = 1/2$ and, therefore, $\nu_{in} = 1$ and $\nu_\parallel = 1/2$ according to (3.22) and (3.24), while an expansion around $d = 2+d_\perp = \infty$ yields /35/ $\nu_{in} \approx d/2$, $\nu_{cr} \approx 1 - 1/d$ and, thus, $\nu_\parallel \approx d/2$

E. Singular free energy arising from thermal fluctuations.

The fluctuations of a *rough* manifold give a contribution, F_{FL}, to its free energy. Consider a manifold segment of linear (intrinsic) size, L_{in}. Its largest humps then have a lateral and

transverse extension $L_{\parallel} \sim L_{in}$ and $L_{\perp} \sim L_{in}^{\zeta}$, respectively, see (3.5) and Fig. 1(a). The thermal free energy, F_{FL}, of such a hump should be of order $\sim T$ as suggested by the equipartition theorem. Therefore, the thermal free energy per unit area is given by /1/

$$f_{FL} = F_{FL}/L_{in}^{d\parallel} \simeq T/L_{in}^{d\parallel} \simeq 1/L_{\parallel}^{d\parallel} \sim 1/L_{\perp}^{\tau} \qquad \text{with } \tau = d_{\parallel}/\zeta \ . \qquad (3.25)$$

Now, assume that the manifold is confined in such a way that its largest humps are characterized by an intrinsic scale, ξ_{in}, and two extrinsic scales, $\xi_{\parallel} \sim \xi_{in}$ and $\xi_{\perp} \sim \xi_{in}^{\zeta}$ Such a behavior occurs, e.g., close to a roughening transition (with $\zeta = \zeta_r$), see Fig. 2(a). Similar manifold states characterize the unbinding of manifolds as in wetting, adhesion, and adsorption phenomena as will be explained in Sec. V, see Fig.5(a) below. In these cases, the manifold can be viewed as an ensemble of essentially uncorrelated humps. Thus, a manifold of linear size, $L_{in} \sim L_{\parallel}$, consists of $(L_{in}/\xi_{in})^{d\parallel} \sim (L_{\parallel}/\xi_{\parallel})^{d\parallel}$ independent humps. The thermal free energy of each hump should again be $\sim T$. This leads to $F_{FL} \simeq T(L_{in}/\xi_{in})^{d\parallel}$, and the thermal free energy per unit area arising from the fluctuations is now given by /4/

$$f_{FL} \simeq T/\xi_{in}^{d\parallel} \simeq T/\xi_{\parallel}^{d\parallel} \sim 1/\xi_{\perp}^{\tau} \qquad \text{with} \quad \tau = d_{\parallel}/\zeta \qquad \text{for } \textit{rough} \text{ states} \qquad (3.26)$$

as in (3.25). The first relation, $f_{FL} \sim 1/\xi_{in}^{d\parallel}$, is the socalled *hyperscaling* relation. For example, a power law behavior, $\xi_{in} \sim \xi_{\parallel} \sim (T_*-T)^{-\nu\parallel}$, as in (3.18) implies

$$f_{FL} \sim (T_*-T)^{2-\alpha} \quad \text{with} \quad 2-\alpha = d_{\parallel} \, \nu_{\parallel} = d_{\parallel} \, \nu_{in} \ . \qquad (3.27)$$

For *crumpled* manifolds, the free energy arising from thermal fluctuations exhibits very similar behavior. Thus, a manifold segment of linear (intrinsic) size, L_{in}, forms large blobs of extrinsic size $L_{\perp} \sim L_{\parallel} \sim L_{in}^{\nu}$, see (3.17) and Fig. 1(b), which again give rise to a thermal free energy, $F_{FL} \simeq T$. This implies that the thermal free energy per unit (intrinsic) area is given by

$$f_{FL} = F_{FL}/L_{in}^{d\parallel} \simeq T/L_{in}^{d\parallel} \sim 1/L_{\parallel}^{\tau} \sim 1/L_{\perp}^{\tau} \qquad \text{with} \quad \tau = d_{\parallel}/\nu \ . \qquad (3.28)$$

In the presence of some external constraint, the large-scale configurations of a crumpled manifold can be regarded as an ensemble of statistically independent blobs with $\xi_{\perp} \sim \xi_{\parallel} \sim \xi_{in}^{\nu}$, see Fig. 2(b) above and Fig. 5(b) below. Each blob has a free energy $\sim T$. Then, a manifold of linear size, L_{in}, has a free energy $F_{FL} \simeq T(L_{in}/\xi_{in})^{d\parallel}$ since $(L_{in}/\xi_{in})^{d\parallel}$ is the number of blobs. Therefore, the free energy per unit (intrinsic) area arising from the thermal

fluctuations scales as /36,4/

$$f_{FL} \simeq T/\xi_{in}^{d\|} \sim 1/\xi_{\|}^{\tau} \sim 1/\xi_{\perp}^{\tau} \quad \text{with} \quad \tau = d_{\|}/\nu \quad \text{for } \textit{crumpled} \text{ states} \tag{3.29}$$

as in (3.28). The first relation can again be regarded as hyperscaling. Thus, if $\xi_{in} \sim (T_*-T)^{-\nu_{in}}$, the free energy has a singular part $f_{FL} \sim (T_*-T)^{2-\alpha}$ with $2-\alpha = d_{\|} \nu_{in}$

IV. INTERFACES IN (IDEAL) QUASIPERIODIC SYSTEMS.

A. Penrose tiling and quasiperiodic interface potentials of entropic origin.

A few years ago, a new class of crystalline materials has been discovered which exhibit sharp diffraction peaks and five-fold symmetry axes. /37/ Such a symmetry is, however, not compatible with a periodic structure which is built up from a single unit cell. It is now generally believed that these materials represent *quasicrystals* which are built up from two (or more) unit cells which are arranged in a quasiperiodic manner. The simplest models for such structures are provided by 2-dim Penrose tilings which are built up from two different tiles, namely a thin and thick rhombus, see Fig. 3. /37/ These tilings exhibit orientational long-range order with a five-fold symmetry axis since all edges point in one out of five possible directions.
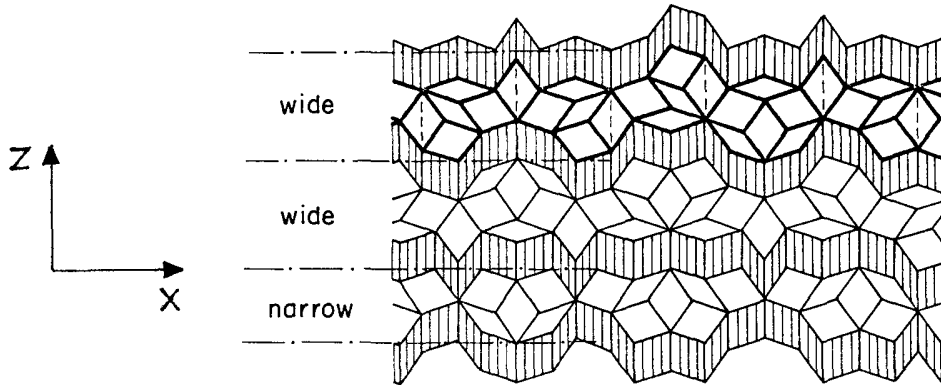
Fig.3:   2-dim Penrose tiling : the shaded rows separate wide (W) and narrow (N) lanes.

Next, consider an Ising (or lattice gas) model on such a Penrose-tiling: on each tile, an Ising spin, $S_i = \pm 1$, is placed. Each spin interacts with four nearest neighbors on four adjacent tiles. The coupling constant, $J/2$, is taken to be ferromagnetic. Then, an interface separating an up-spin domain from a down-spin domain runs along the edges of the tiling. At $T = 0$, the interfacial configurations with the lowest energy have normal vectors which are parallel to one of the five possible edge orientations. /15,16/ In the following, I focus on one such orientation and choose the x- and the z-axis to be perpendicular and parallel to

this orientation, see Fig. 3.

The tiling shown in Fig. 3 has been decomposed into (unshaded) lanes and shaded rows. /15/ The rows contain all tiles with two edges parallel to the z-axis while all other tiles are contained within the lanes. It turns out that all interfacial configurations, which stay within a given lane and which connect two vertices within this lane, have the same length and, thus, the same energy (provided there are no overhangs). Thus, the interfacial groundstate is degenerate at $T = 0$. For an interface consisting of M segments (or edges), this degeneracy behaves as $g_M \sim \exp(MS)$ for large M. There are essentially two types of lanes, narrow (N) and wide (W) ones, see Fig. 3, which have a ground state entropy per segment $S_N \simeq 0.45$ and $S_W \simeq 0.54$, respectively. /15,16/ These two types of lanes form a Fibonacci-sequence.

The Fibonacci-sequence of the two elements W and N can be expressed in terms of the function $f(z)$ with $f(z) = W$ for $0 \leq z \leq 1$, $f(z) = N$ for $1 \leq z < \sigma = (1+\sqrt{5})/2$, and $f(z+\sigma) = f(z)$ for all real z. The Fibonacci sequence of W and N is then given by the sequence $f(z=n)$ for integer $n = 0, \pm 1, \ldots$. Here, n is a discrete height variable which counts the number of lanes between the interface and the x-axis. Likewise, the ground state entropy (per segment) of the lane with height n is given by $S(z=n)$ with $S(z) = S_W$ for $0 \leq z < 1$, $S(z) = S_N$ for $1 \leq z < \sigma$ and $S(z+\sigma) = S(z)$

At low $T > 0$, the interface makes many steps within a lane before it hops across a row into a neighboring lane. Furthermore, it prefers to stay in the wide lanes since it can then increase its configurational entropy. Therefore, the interface feels an effective quasiperiodic potential, $V_{QP}(z=n)$, with

$$
\begin{aligned}
V_{QP}(z) &= 0 && \text{for} && 0 \leq z < 1 \\
&= T(S_W - S_N) && \text{for} && 1 \leq z < \sigma \quad,
\end{aligned}
\tag{4.1}
$$

and $V_{QP}(z+\sigma) = V_{QP}(z)$, which is *of entropic origin.* For higher temperatures, the precise form of $V_{QP}(z=n)$ within the Penrose tiling will be more complicated but it will still be quasiperiodic.

B. Interfacial behavoir in $d = 1+1$

Inside the lanes, the interface feels a quasiperiodic potential as in (4.1). When it hops across a row, it has to increase its length by one edge and, thus, its energy by twice the nearest-neighbor coupling of the Ising model. Thus, the main effect of the Penrose tiling on the interface should be captured by the effective Hamiltonian

$$
\mathscr{H}\{z\}/T = \sum_{<ij>} (J/T)|z_i - z_j| + \sum V_{QP}(z_i)/T
\tag{4.2}
$$

for the discrete height variable $z_i \equiv z(x_i)$ where x_i labels the sites of a 1-dim lattice.

1. Transfer matrix approach.

Now, assume that the interface has the fixed height $z = 0$ at $x = 0$ and consider the total weight or probability, $P(x,z)$, to find the interface at $z(x_N) = z$. For the 1-dim model as given by (4.2) which contains only nearest-neighbor couplings, $P(x=x_N,z)$ depends only on $P(x=x_{N-1},z')$ for the previous step. The associated transfer matrix can be symmetrized by the change of variable, $W(x,z) \equiv \exp[\frac{1}{2} V_{QP}(z)]\, P(x,z)$. Furthermore, it is convenient to use the restriction $|z_i - z_j| = 0$ or 1. Then, the weight evolves according to /15/

$$W(x+1,z) - W(x,z) = -\mathscr{S}W(x,z) \qquad (4.3)$$

with the Schrödinger-type operator

$$\mathscr{S}W(x,z) \equiv -e^{-J/T}\,[t(z,z+1)\,W(x,z+1) + t(z,z-1)\,W(x,z-1)] + U(z)\,W(x,z) \quad , \qquad (4.4)$$

the potential

$$U(z) \equiv 1 - exp[-V_{QP}(z)/T] \quad , \qquad (4.5)$$

and the 'hopping' coefficients

$$t(z,z') \equiv exp[-\tfrac{1}{2}\{V_{QP}(z) + V_{QP}(z')\}/T] = [1 - U(z)]^{1/2}\,[1 - U(z')]^{1/2} \quad . \qquad (4.6)$$

Since the operator $\mathscr{S}$ is symmetric, its eigenvalues, E, are real. Then, the weight $W(x,z)$ may be expressed in terms of the eigenfunctions $\phi_E(z)$ according to

$$W(x,z) = \frac{1}{N}\int d\mu(E)\, e^{-(E-E_0)x}\, C_E\, \phi_E(z) \qquad (4.7)$$

as follows from (4.3) in the continuum limit, $W(x+1,z) - W(x,z) \approx \partial W/\partial x$.

2. Interfacial roughness and coherence length ξ_c

As discussed in Sec.III.A, the fluctuations of an interface can be characterized by the difference correlation function, ΔC_z, as defined in (3.2). In the present context, one has $L_\perp^2 = \Delta C_z(L_\parallel) = \frac{1}{2}\sum W(L_\parallel,z)\,z^2$. Thus, $L_\perp$ measures the width of the weight function W. For large $L_\parallel$, W is governed by the eigenfunctions $\phi_E(z)$ close to the groundstate. Indeed, inspection of (4.7) shows that, for large $x = L_\parallel$, only eigenfunctions with $E \lesssim E_1$ and

$$E_1 - E_0 \sim 1/L_\parallel \qquad (4.8)$$

contribute to the weight $W(L_\parallel,z)$ because of the exponential factor $\sim exp[-(E-E_0)L_\parallel]$

If the eigenstates close to the groundstate, ϕ_{E_0}, are *localized,* the probability $W(L_\parallel,z)$ will

attain a stationary distribution for large $L_{\parallel}$, and the interface is *smooth*. A *rough* interface, on the other hand, corresponds to the situation where the ground state and the eigenstates close to it are *extended*. In the latter case, the width, $L_{\perp}$, of $W(L_{\parallel}, z)$ can be estimated by /15/

$$L_{\perp} \sim \xi_c(E_1, E_0) \tag{4.9}$$

where ξ_c is the *coherence length* of the eigenstates $\phi_{E_1}(z)$ and $\phi_{E_0}(z)$ with E_1 defined by (4.8). For $z \ll \xi_c$, the two states look indistinguishable (apart from an overall prefactor).

3. Coherence length and integrated density of states.

As E_1 approaches E_0, the coherence length ξ_c must diverge (provided the states are extended as assumed). It turns out that the singular behavior of ξ_c is intimately related to the scaling behavior of the integrated density of states. In order to understand this relation, consider the Schrödinger-type operator $\mathscr{S}$ as given by (4.4)-(4.6) but with constant hopping coefficients $t(z,z') = 1$. Then, one has to study the eigenvalue problem

$$-e^{-J/T}[\phi_E(z+1) + \phi_E(z-1)] + U(z|\sigma)\,\phi_E(z) = E\,\phi_E(z). \tag{4.10}$$

The potential $U(z|\sigma)$ is quasiperiodic and satisfies $U(z+\sigma|\sigma) = U(z|\sigma)$ for real z where σ is an irrational number such as the golden mean.

The spectrum of a quasiperiodic potential as in (4.10) can be determined numerically from a sequence of *rational approximants,* $U^{(m)}(z) \equiv U(z|\sigma^{(m)})$ with $\sigma^{(m)} = p^{(m)}/q^{(m)} \approx \sigma$ for large m where $p^{(m)}$ and $q^{(m)}$ are integers, see e.g. Ref. /38/. The m–th approximant, $U^{(m)}(z)$, has period $p^{(m)}$. One then has a Bloch theorem and the spectrum of $U^{(m)}(z)$ consists of $p^{(m)}$ bands where each band has the same number of states,

$$\mathscr{D}^{(m)} \sim 1/p^{(m)} \quad . \tag{4.11}$$

Furthermore, numerical calculations have shown that the band widths, $\Delta E^{(m)}$, shrink according to /38/

$$\Delta E^{(m)} \sim [1/p^{(m)}]^{1/\alpha(E_<)} \tag{4.12}$$

for large m where $E_<$ is the lower edge of the band of eigenvalues.

Now, consider a large but fixed value for the longitudinal extension, $L_{\parallel}$, of the interface, which implies a small energy gap $E_1 - E_0 \sim 1/L_{\parallel}$ as in (4.11). As long as this energy gap satisfies $E_1 - E_0 \ll \Delta E^{(m)}$, the eigenstates ϕ_{E_1} and ϕ_{E_0} are *coherent* over the period $p^{(m)}$ of the potential $U^{(m)}(z)$. For $E_1 - E_0 \gg \Delta E^{(m)}$, on the other hand, the two states are separated by many band edges at which the states undergo a phase shift, and thus are

incoherent over the period $p^{(m)}$. Therefore, one can estimate the coherence length, ξ_c, by

$$\xi_c(E_1, E_0) \sim p^{(M)} \quad \text{with} \quad E_1 - E_0 \sim \Delta E^{(M)} \tag{4.13}$$

where the lower band edge of $\Delta E^{(M)}$ is now the groundstate energy : $E_< = E_0$

It then follows from (4.11) and (4.12) that the total number of states, $\mathscr{D}^{(M)}$, in the lowest band is $\mathscr{D}^{(M)} \sim 1/p^{(M)} \sim [\Delta E^{(M)}]^{\alpha(E_0)}$. This together with (4.13) implies that the integrated density of states has the asymptotic behavior $\mathscr{D}(E_1) - \mathscr{D}(E_0) \sim (E_1 - E_0)^{\alpha(E_0)}$ in the limit of small $E_1 - E_0$ as has been numerically found in many studies. In the same way, one concludes that the coherence length behaves as /15/

$$\xi_c(E_1, E_0) \sim (E_1 - E_0)^{-\alpha(E_0)} \tag{4.14}$$

for small $E_1 - E_0$. Thus, the divergence of ξ_c is governed by the same exponent as the decay of the integrated density of states.

4. Roughness exponent ζ.

The various scaling arguments described in the previous subsections can now be combined in order to obtain a relation between the interfacial roughness, $L_\perp$, and the (projected) length, $L_\parallel$, of the interface. Indeed, a combination of (4.9), (4.14), and (4.8) leads to

$$L_\perp \sim \xi_c(E_1, E_0) \sim (E_1 - E_0)^{-\alpha(E_0)} \sim L_\parallel^{\alpha(E_0)} \quad . \tag{4.15}$$

This means that the *roughness exponent, ζ,* as defined by (3.3)-(3.5), is given by /15/

$$\zeta = \alpha(E_0) \tag{4.16}$$

where $\alpha(E_0)$ governs the decay of the integrated density of states at the ground state.

As a first example, consider the interface Hamiltonian (4.2) with the restriction $|z_i - z_j| = 0$ or 1 as suggested by the Penrose tiling for low T. It then follows from (4.1) and (4.5) that the quasiperiodic potential $U(z|\sigma)$ has the form

$$
\begin{aligned}
U(z|\sigma) \quad &= 0 & \text{for } 0 \leq z < 1 \\
&= U_N \equiv 1 - exp[S_N - S_W] & \text{for } 1 \leq z < \sigma = (1+\sqrt{5})/2
\end{aligned}
\tag{4.17}
$$

In the following, this case will be referred to as the *Fibonacci potential.* If one includes only the leading term, $t(z,z') \approx 1$, of the hopping coefficients (valid for small U), one has to calculate the E-spectrum of (4.10) with $U(z|\sigma)$ as given by (4.17). This can be done

analytically using methods of nonlinear dynamics. As a result, one finds the exponent $\alpha(E)$ for the integrated density of states /39/ and, thus, the roughness exponent /15/

$$\zeta = \alpha(E_0) = ln[\ (1+\sqrt{5})/2\ ]\ /\ ln\ \delta \tag{4.18}$$

with

$$\delta = \tfrac{1}{2}[K_I + (K_I^2 + 4)^{1/2}]\ \ \text{and}\ \ K_I = (25 + 4e^{2J/T}\ U_N^2)^{1/4}\ \ . \tag{4.19}$$

This implies $\zeta < \tfrac{1}{2}$ for all parameter values and /15,16/

$$\zeta \approx 2\ ln[\ (1+\sqrt{5})/2\ ]\ (T/J)\quad \text{for}\quad \text{small T/J} . \tag{4.20}$$

The nonlinear dynamics approach can be generalized to handle the case of general hopping coefficients $t(z,z+1) = t_{WW}$ or t_{WN} as in the model defined by (4.2) and (4.1). The resulting expression for $\zeta = \alpha(E_0)$ is slightly more complicated and now explicitly depends on E_0. /15/ However, the inequality $\zeta < \tfrac{1}{2}$ and the low-T behavior (4.20) are still valid.

Thus, for the Fibonacci-potential as given by (4.17), the roughness exponent ζ is found to be *nonuniversal,* i.e., to depend on the parameters of the system. This nonuniversality arises from the fact that the eigenstates close to the groundstate are *critical scattering states.* Such states are self-similar and form the singularly continuous part of the spectrum.

Quite generally, the character of the low-lying eigenstates will determine the value of the roughness exponent ζ as is evident from the preceding discussion. Three cases must be distinguished: (i) these states are *localized* corresponding to a smooth interface and, thus, $\zeta = 0$; (ii) these states are *normal scattering* states which implies a rough interface with the *universal* exponent $\zeta = 1/2$; and (iii) the states close to the groundstate are *critical scattering states* which leads to nonuniversal values for ζ.

5. Roughening transitions in $d = 1+1$

For some quasiperiodic systems, the character of the low-lying states close to the ground state changes as a function of temperature (or any other parameter). Thus, these states may be localized for some values of the parameters but extended for others. Such a behavior was found for the 1-dim almost Mathieu (or Harpers) potential. For electrons moving in such a potential, this implies a metal-insulator transition. /40/ In the present context, such a behavior leads to a *roughening transition* from a smooth to rough state of the interface at some roughening temperature, $T = T_r$. /15/

The almost-Mathieu (or Harpers) potential has the form

$$U(z|\sigma) = -U\ cos[2\pi z/\sigma]\quad \text{with}\ \ U > 0 \tag{4.21}$$

and $\sigma = (1+\sqrt{5})/2$. The choice $U > 0$ ensures that the global minimum of $U(z)$ is at $z = 0$

The corresponding eigenvalue problem as given by (4.10) remains unchanged under a duality transformation with $\tilde{U} \equiv U \; exp(J/T) \to 4/\tilde{U}$. /40/ If there is a unique transition, it must then occur at the self-dual point

$$\tilde{U}_* = (e^{J/T}U)_* = 2 \quad . \tag{4.22}$$

Now, consider the interface model (4.2) with the restriction $|z_i - z_j| = 0$ or 1 and with $V_{QP}(z)/T = U(z|\sigma)$ as given by (4.21). One then has to study the Schrödinger-type equation (4.4)-(4.6) which, in the limit of small U, reduces to the form (4.10). It then follows from (4.22) that the interface undergoes a roughening transition at a roughening temperature $T = T_r$ which behaves as /15/

$$T_r \approx J / ln(2/U) \quad \text{for small } U \quad . \tag{4.23}$$

For constant hopping coefficients as in (4.10), the roughening exponent ζ can be obtained, via (4.16), from numerical studies of the density of states /38/. One then finds that /15/

$$\begin{aligned}
\zeta \; &= \; \zeta_r \simeq 0.421 \quad \text{for} \quad T = T_r \quad (\text{or } \tilde{U} = 2) \\
&= 1/2 \qquad \text{for} \quad T > T_r \quad (\text{or } \tilde{U} < 2) \; .
\end{aligned} \tag{4.24}$$

For $\tilde{U} > 2$, the eigenstates are exponentially localized with a localization length $\sim 1/ln(\tilde{U}/2)$ which diverges as $\tilde{U}_* = 2$ is approached from above. /40/ This implies that the interfacial roughness, $\xi_\perp$, behaves as $\xi_\perp \sim (T_r - T)^{-\nu_\perp}$ with $\nu_\perp = 1$ as the roughening temperature, T_r, is approached from below. It then follows from the general scaling relation (3.19) (and $\zeta_r > 0$) that the parallel correlaction length, $\xi_{||}$, behaves as $\xi_{||} \sim (T_r - T)^{-\nu_{||}}$ with $\nu_{||} = \nu_\perp/\zeta_r \simeq 2.38$. Likewise, hyperscaling as described in Sec.III.E implies for a rough interface that the singular part of the interfacial free energy, $\Sigma_{FL} \equiv f_{FL} \sim 1/\xi_{||}$. Then, the interfacial specific heat, C_I, has the singular part $\sim d^2\Sigma_{FL}/dT^2$ and behaves as $C_I \sim (T_r - T)^{-\alpha_r}$ with $\alpha_r = 2 - 1/\zeta_r \simeq -0.375$. Thus, the interfacial specific heat exhibits a weak cusp-like singularity at the roughening transition.

This scaling behavior shows that roughening transitions of 1-dim interfaces in quasiperiodic systems are *second-order* transitions and, thus, are very different from the well-known roughening transition in 3-dim periodic systems which are of the Kosterlitz-Thouless type. Furthermore, the critical behavior of the roughening transitions considered here will depend on the details of the quasiperiodic potentials (and hopping coefficients). Similar roughening transitions with somewhat different exponents have been found (i) for a quasiperiodic potential intermediate between the Fibonacci and the

almost-Mathieu potential /30/, and (ii) for interface models in which the interface potential varies quasiperiodically both with z and with x /31/.

C. Interfacial behavior in d = 2+1
1. Continuum model

In d = 2+1, quasiperiodic structures have been constructed by a variety of methods. One important example is the (ideal) icosahedral tiling as generated, e.g., by the dual-grid method. /37/ This tiling is built up from parallelepipeds (or rhombohedra) where each parallelepiped has three out of six possible edge orientations. Such a tiling can be decomposed, for each edge orientation, into a stack of sheets and slabs which are, on average, parallel. /41/ The sheets in d = 2+1 play the role of the rows in d = 1+1 (see Fig. 3) and contain all tiles with four faces parallel to the chosen edge orientation; the slabs play the role of the lanes (see Fig. 3) and are composed of all the remaining tiles.

At T = 0, an interface will be confined to one of the slabs and, thus, will exhibit a finite ground-state entropy. Furthermore, this entropy should vary quasiperiodically from slab to slab. Thus, at T > 0, the interface in d = 2+1 will again feel an effective quasiperiodic potential of entropic origin. In this way, one is led to study the 3-dim analogue of the effective Hamiltonian as given by (4.2) for which the integer height variable, $z(\mathbf{x_i})$, counts the number of slabs perpendicular to a certain edge orientation. This discrete height variable is now replaced by a continuous one which feels a generic quasiperiodic potential such as

$$V_{QP}(z)/T = A_0 \, cos(q_0 \, z) + A_1 \, cos(q_1 \, z) \tag{4.25}$$

with $q_0 \equiv 2\pi/\ell_0$, $q_1 \equiv q_0/\sigma$ and $\sigma = (1+\sqrt{5})/2$. In addition, the discrete lattice, $\mathbf{x_i}$, is replaced by a continuous coordinate $\mathbf{x} = (x_1, x_2)$. Then, the effective Hamiltonian for the interfacial shape has the generic form

$$\mathcal{H}\{z\}/T = \int d^2x \, \{ \tfrac{1}{2} (K/T) \, (\nabla z)^2 + V_{QP}(z)/T \} \tag{4.26}$$

with $V_{QP}(z)$ as given by (4.25). It will be shown below that such a continuum model leads to a smooth interface for all $T < \infty$ and, thus, to a roughening temperature, $T_r = \infty$ /41-43/ This property should also hold for the discrete models and for more realistic models which include a quasiperiodic variation of V_{QP} with $\mathbf{x}$.

The global minimum of the quasiperiodic potential $V_{QP}(z)$ as given by (4.25) depends on the signs of the amplitudes A_0 and A_1. In fact, one could also allow for a phase shift between the two cosine terms such that $cos(q_1 z)$ is replaced by $cos(q_1 z + \Delta)$. Then, the global minimum of $V_{QP}(z)$ will be at $z = \infty$ for most choices of the phase Δ. In such a situation, the interface can only be metastable at finite z, and the interfacial roughness in thermal equilibrium is not a well-defined quantity. Therefore, I chose $\Delta = 0$ in (4.25) and take $A_0 <$

0 and $A_1 < 0$. /41/ This choice ensures that the global minimum is at $z = 0$ for any finite z–interval. This together with the symmetry $V_{QP}(-z) = V_{QP}(z)$ implies $<z> = 0$

2. Functional renormalization and cumulant expansion

The model as defined by (4.26) and (4.25) will now be studied by a functional renormalization group (RG) method. Such a RG method consists of three basic steps. First, the fluctuating field, $z(\mathbf{x})$, is divided up into two parts : $z(\mathbf{x}) = z_<(\mathbf{x}) + z_>(\mathbf{x})$ where $z_<$ and $z_>$ represent the small-wavenumber (or large-scale) and the large-wavenumber (or small-scale) fluctuations. Then, the small-scale fluctuations, $z_>$, are integrated out which gives rise to

$$exp[-\mathcal{H}'\{z_<\}] \equiv \frac{1}{N} \int \mathcal{D}\{z_>\} \; exp[-\mathcal{H}\{z_<+z_>\}] \; . \qquad (4.27)$$

(The factor $1/T$ has been absorbed into $\mathcal{H}$ for notational convenience.) Finally, the spatial coordinate, $\mathbf{x}$, and the fluctuating field, z, are rescaled according to

$$\mathbf{x} \to \mathbf{x}/b \quad \text{and} \quad z \to z/b^\zeta \quad \text{with} \quad b > 1 \quad \text{and} \quad \zeta = 0 \; . \qquad (4.28)$$

Obviously, the most difficult step in the RG is the partial trace over the small-scale fluctuations as in (4.27). In order to perform this step in a perturbative way, let us divide $\mathcal{H}$ into $\mathcal{H}_0\{z\} \equiv \int d^2x \; \frac{1}{2} \; (K/T) \; (\nabla z)^2$ and $\mathcal{H}_1\{z\} \equiv \int d^2x \; V_{QP}(z)/T$. One then has

$$\mathcal{H}\{z_<+z_>\} = \mathcal{H}_0\{z_<\} + \mathcal{H}_0\{z_>\} + \mathcal{H}_1\{z_<+z_>\} \quad . \qquad (4.29)$$

When this expression is inserted into (4.27), one obtains

$$exp[-\mathcal{H}'\{z_<\}] = exp[-\mathcal{H}_0\{z_<\}] \; < exp[-\mathcal{H}_1\{z_<+z_>\}] > \qquad (4.30)$$

where the expectation value, $<...>$, is calculated with the harmonic weight, $exp[-\mathcal{H}_0\{z_>\}]$

Now, *assume* that the interface undergoes a roughening transition at a finite roughening temperature, $T = T_r < \infty$. Then, for $T > T_r$, the quasiperiodic potential, V_{QP} must be *irrelevant* and must eventually become *small* unter the RG transformation. Thus, in order to study the rough phase, one may perform an expansion of (4.30) in powers of V_{QP} or $\mathcal{H}_1$ This leads to the cumulant expansion as given by

$$< exp[-\mathcal{H}_1] > = exp[\sum \frac{1}{n!} <(-\mathcal{H}_1)^n>_c] \approx exp[-<\mathcal{H}_1> + \frac{1}{2} <\mathcal{H}_1\mathcal{H}_1>_c] \qquad (4.31)$$

where the subscript c stands for cumulant. It then follows from (4.30) that, apart from the rescaling transformation (4.28), the renormalized Hamiltonian is given by

$$\mathcal{H}'\{z_<\} \approx \mathcal{H}_0\{z_<\} + < \mathcal{H}_1\{z_<+z_>\} > - \tfrac{1}{2} < \mathcal{H}_1\{z_<+z_>\} \, \mathcal{H}_1\{z_<+z_>\} >_c \quad (4.32)$$

3. Cumulant expansion up to second order in $\mathcal{H}_1$

The first-order term of the cumulant expansion for the quasiperiodic potential (4.25) is

$$< \mathcal{H}_1\{z_<+z_>\} > \; = \; \int d^2x \, [\, A_0 < cos[q_0(z_<+z_>)]> + A_1 < cos[q_1(z_<+z_>)]> \,] \quad (4.33)$$

The expectation values which involve the harmonic weight $exp[-\mathcal{H}_0\{z_>\}]$ are easily calculated. The result is $<cos[q_j(z_<+z_>)]> = cos[q_j z_<] \, exp[-\tfrac{1}{2}q_j^2 <z_>^2>]$. In addition, rescaling as in (4.28) yields a factor b^2. Therefore, the renormalized amplitudes are

$$A_j' = A_j \, b^2 \, exp[\, -\tfrac{1}{2} \, q_j^2 < z_>^2 >] \quad . \quad (4.34)$$

Since $<z_>^2> = (T/K)c(b)$, one has $A_j' = A_j$ at $T = T_r(q_j)$ with

$$T_r(q_j)/K = \; 4 \, ln[b] \, / \, c(b) \, q_j^2 \approx 8\pi \, / \, q_j^2 \quad \text{for} \quad b \to 1 + \Delta s \, . \quad (4.35)$$

Thus, to leading order in the cumulant expansion, the potential term $A_j \, cos[q_j z]$ is relevant and irrelevant for $T < T_r(q_j)$ and $T > T_r(q_j)$, respectively.

Therefore, starting with two components of V_{QP} as in (4.25), one concludes that both components are irrelevant for $T > T_r(q_1)$. However, this does *not* represent the roughening temperature of the system since higher-order terms of the RG *generate* additional components of V_{QP} which have *smaller* wavenumbers q_j and, thus, *higher* temperatures $T_r(q_j)$ according to (4.35). Even though the second-order calculation is straight forward, the details are somewhat tedious and I will only indicate its main ingredients.

The additional relevant components of the potential arise from the cross term

$$V_2(q_0,q_1) \equiv \; < \int d^2x_0 \, A_0 \, cos[q_0 z(\mathbf{x}_0)] \int d^2x_1 \, A_1 \, cos[q_1 z(\mathbf{x}_1)] >_c \quad (4.36)$$

The main contribution to the integrations comes from $\mathbf{x}_0 \simeq \mathbf{x}_1$. To leading order in a gradient expansion, one then obtains

$$V_2(q_0,q_1) \approx \int d^2x \, A_0 A_1 \{ g_+ \, cos[(q_0+q_1)z_<] + g_- \, cos[(q_0-q_1)z_<] \} \quad (4.37)$$

with parameter-dependent coefficients $g_\pm$. The first term $\sim cos[(q_0+q_1)z]$ has a larger wavenumber and, thus, is irrelevant for $T \geq T_r(q_1)$. However, the second term in (4.37) has

the wavenumber $q_2 \equiv q_0 - q_1 = q_0 (1-1/\sigma) = q_0 / \sigma^2$ with $\sigma = (1+\sqrt{5})/2$ which is smaller than both q_0 and $q_1 = q_0/\sigma$. It then follows from (4.35) that this term is relevant up to $T_r(q_2) > T_r(q_1)$

Now, further iterations of the RG transformation generate components with smaller and smaller wavenumbers. Indeed, it is not difficult to see that the (j–1)th iteration step generates a term $A_j cos[q_j z]$ with $q_j = (q_{j-2} - q_{j-1}) = q_0/\sigma^j$ which is relevant up to $T = T_r(q_j) \sim \sigma^{2j}$ according to (4.35). Therefore, for any finite T, the interface feels an effective quasiperiodic potential on sufficiently large scales. This implies a *smooth* interface at $T < \infty$ and an *infinite roughening temperature,* $T_r = \infty$. /41-43/ This prediction of the RG has been confirmed by recent Monte Carlo simulations. /44/

V. INTERACTIONS OF MANIFOLDS AND UNBINDING TRANSITIONS

A. Wetting, Adhesion, and Adsorption Phenomena

A variety of physical phenomena is governed by the mutual interaction of interfaces, membranes, and polymers. /4/ The geometry of such phenomena is shown in Fig. 4. *Wetting* phenomena occur when an interface between two macroscopic bulk phases contains a thin film or layer of a third phase, see Fig. 4(a). /45/ The intermediate layer is bounded by two interfaces, and its thickness is determined by the mutual interactions of these interfaces. *Adhesion* of an oriented membrane onto an interface is shown in Fig. 4(b). This membrane could be, e.g., a small segment of a large lipid vesicle which adheres to the interface. *Adsorption* of a polymer and of a crumpled membrane is shown in Fig. 4(c) and 4(d).
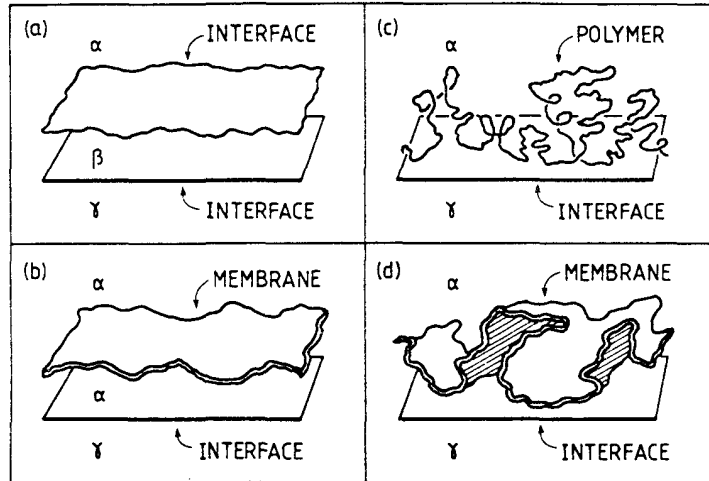
Fig.4:   Bound states of low-dim manifolds : (a) Wetting, surface melting and related phenomena; (b) Adhesion of an oriented membrane; and (c),(d) Adsorption of a polymer and a crumpled membrane. (α, β, and γ denote distinct phases)

The manifolds shown in Fig. 4 form *bound states* in the sense that their mean separation has a finite value. These states require the presence of some *attractive* interaction between the manifolds. For a given shape of the interfaces, membranes, or polymers, their mutual interaction directly reflects microscopic intermolecular forces. This *direct* interaction consists of several short-ranged and long-ranged contributions such as electrostatic, van der Waals or structural interactions. There is in fact a huge literature on intermolecular forces and the resulting direct interactions. However, it has been realized only recently that these *interactions are strongly renormalized by shape fluctuations.*

Quite generally, the renormalization arising from shape fluctuations acts to decrease the attractive part of the direct interaction and to increase its repulsive part. Now, consider the case of thermally-excited fluctuations. At low T, these fluctuations are weak and the renormalized interaction closely resembles the direct interaction. However, as T is increased, the renormalization becomes more and more effective up to a characteristic unbinding temperature, $T = T_u$. For $T > T_u$, the renormalized interaction no longer has an attractive part, and the two manifolds are completely unbound.

As T_u is approached from below, the system undergoes an *unbinding transition* : the mean separation, ℓ, of the manifolds goes to infinity and typically behaves as $\ell \sim (T_u - T)^{-\psi}$. The critical exponent ψ depends, to some extent, on the form of the direct interaction, V_{DI}. In fact, one must distinguish several scaling regimes or universality classes for V_{DI}. This can be understood in a rather simple way if the manifolds are again described in terms of humps and blobs, compare Figs. 1 and 2. In the present context, these scaling pictures lead to effective fluctuation-induced interactions.

B. Fluctuation-induced Interactions

First, consider a *rough* manifold bound to a smooth one as in Fig. 4(a) and 4(b). Then, the manifold can again be viewed as an ensemble of essentially uncorrelated humps, see Fig. 5(a). Each hump with intrinsic size, ξ_{in}, has a lateral and transverse extension $\xi_{\parallel} \sim \xi_{in}$ and $\xi_{\perp} \sim \xi_{in}^{\zeta}$, respectively. Then, the scaling arguments of Sec. III.E.1 lead to a singular contribution of the free energy per unit area which is given by /14,46,1/

$$V_{FL} \equiv f_{FL} \sim 1/\xi_{\perp}^{\tau} \quad \text{with} \quad \tau = d_{\parallel}/\zeta \tag{5.1}$$

as in (3.27).

Likewise, a *crumpled* manifold bound to a smooth one can be regarded as an ensemble of essentially uncorrelated blobs, see Fig. 5(b). Each blob with intrinsic size, ξ_{in}, has an extrinsic size $\xi_{\perp} \sim \xi_{\parallel} \sim \xi_{in}^{\nu}$. Now, the scaling arguments of Sec. III.E.2 lead to a free energy per unit (intrinsic) area which behaves as /36,4/

$$V_{FL} \equiv f_{FL} \sim 1/\xi_{\perp}^{\tau} \quad \text{with} \quad \tau = d_{\parallel}/\nu , \tag{5.2}$$

compare with (3.31).

The free energies V_{FL} as given by (5.1) and (5.2) represent *excess* free energies of the *bound* manifolds. Therefore, they may be interpreted as effective, *fluctuation-induced* interactions. These interactions have two important properties: (i) they are *repulsive* and, thus, act to drive the manifolds apart; and (ii) they are *long-ranged* (for $\zeta > 0$ and $\nu > 0$) and, thus, may compete even with long-ranged components of the direct interactions.
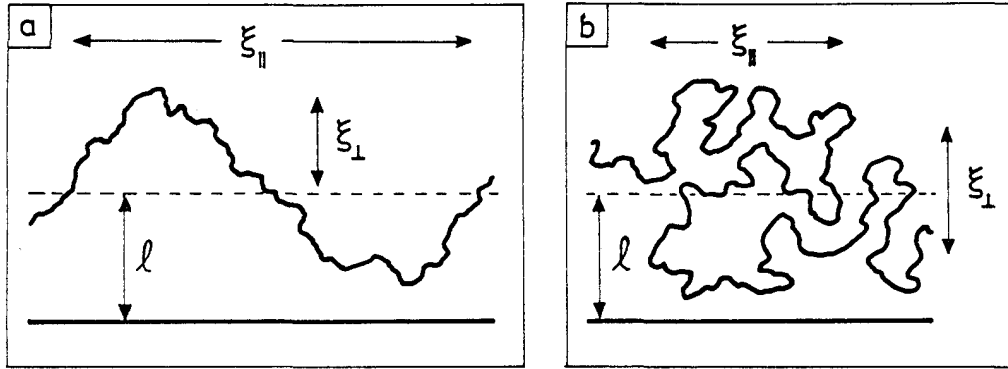
Fig.5: (a) A *rough* manifold with $\xi_\perp \sim \xi_\parallel{}^\zeta \sim \xi_{in}^\zeta$, and (b) a *crumpled* manifold with $\xi_\perp \sim \xi_\parallel \sim \xi_{in}^\nu$, which are bound to a smooth manifold at mean separation ℓ.

C. Different Scaling Regimes

Now, the fluctuation-induced interaction will be compared with the direct interaction arising from intermolecular forces. For the geometries as shown in Fig. 4, this direct interaction, V_{DI}, depends on the coordinate z which measures the distance of the fluctuating manifold from the smooth interface. Then, the interaction free energy (per unit area) of the bound manifold can be estimated by

$$< V_{DI}(z) > \sim V_{DI}(\ell) \quad \text{with} \quad \ell \equiv < z > . \tag{5.3}$$

Now, consider a certain pair of manifolds characterized by a certain value of τ and, thus, by the fluctuation-induced interaction $V_{FL} \sim 1/\xi_\perp^\tau$. Then, the space of all possible direct interactions, V_{DI}, consists of four different scaling regimes. These regimes can be identified by a simple superposition of V_{FL} and V_{DI}. One then finds the following four regimes /1,4/: (i) The *mean-field* (MF) regime characterized by

$$V_{DR}(\ell) \gg V_{FL}(\ell) \sim 1/\ell^\tau \quad \text{for large } \ell . \tag{5.4}$$

where V_{DR} represents the *repulsive* part of V_{DI}. In this situation, the mean separation, ℓ, of the manifolds is not affected by the shape fluctuations; (ii) The *weak-fluctuation* (WFL)

regime defined by

$$V_{DR}(\ell) \ll V_{FL}(\ell) \sim 1/\ell^{\tau} \ll V_{DA}(\ell) \quad \text{for large } \ell \qquad (5.5)$$

where V_{DA} represents the *attractive* part of V_{DI}. The critical behavior within this regime can be obtained in a rather simple way by minimization of $V_{FL} + V_{DI}$; (iii) The *intermediate-fluctuation* (IFL) regime with

$$|V_{DI}(\ell)| \sim V_{FL}(\ell) \sim 1/\ell^{\tau} \quad \text{for large } \ell \ . \qquad (5.6)$$

In this case, the superposition Ansatz indicates that the critical behavior depends both on the long-ranged tail $\sim 1/\ell^{\tau}$ and on the short-ranged part of $V_{DI}(\ell)$; and (iv) The *strong-fluctuation* (SFL) regime characterized by sufficiently short-ranged interactions with

$$|V_{DI}(\ell)| \ll V_{FL}(\ell) \sim 1/\ell^{\tau} \quad \text{for large } \ell . \qquad (5.7)$$

In this regime, the superposition Ansatz predicts a first-order transition while the transition is, in fact, often continuous and then governed by characteristic critical exponents.

The classification as given by eqs. (5.4) - (5.7) which has been obtained from the superposition of direct and fluctuation- induced interactions is fully confirmed by more systematic methods. On the other hand, the superposition Ansatz fails for the critical behavior within the IFL and the SFL regimes. As explained below, functional renormalization group (RG) methods reveal that the critical behavior within these regimes is, in fact, rather unusual.

D.   Renormalized Interactions
1. Functional renormalization : nonperturbative methods

To proceed, let us again consider the geometry displayed in Figs. 4(a) and 4(b). As before, the shape of the fluctuating manifold will be parametrized by $z = z(\mathbf{x})$ where $\mathbf{x}$ is a $d_{\parallel}$—dim coordinate parallel to the smooth interface. The effective Hamiltonian then has the generic form

$$\mathscr{H}\{z\} = \int d^{d\parallel}x \ \{ \tfrac{1}{2} K \ (\nabla^{n}z)^{2} + V_{DI}(z) \} \qquad (5.8)$$

with $n = \zeta + d_{\parallel}/2$ as in (3.7), and an implicit small-distance cutoff, $\mathbf{a}$. The first term in (5.8) describes the elastic energy associated with the shape fluctuations, compare (3.6), while the second term represents the direct interactions of the manifolds. The statistical properties which follow from this model can be studied by a variety of theoretical methods. So far, the most useful approach has been functional renormalization of the direct interaction, V_{DI}

In the context of roughening transitions, functional renormalization of the lattice potential, V_{QP}, can be based on a cumulant expansion in powers of V_{QP}, see Sec. IV.C.

For unbinding phenomena, such a perturbative approach is, however, *not* reliable in general since the direct interaction, $V_{DI}(z)$, contains a hard wall at $z = 0$. Indeed, the RG transformations for V_{DI}, which are discussed below, are *non*perturbative.

The first such method which has been used represents an extension /47,46/ of Wilson's approximate recursion relations /48/. For infinitesimal rescaling factor $b \rightarrow 1 + \Delta s$, this functional RG leads to the nonlinear flow equation /46/

$$\partial V/\partial s = d_{\parallel} V + \zeta z \partial V/\partial z + \tfrac{1}{2} v \, ln[1 + (a_{\perp}^2/v) \, \partial^2 V/\partial z^2] \qquad (5.9)$$

for the renormalized interactions $V(z|s)$ with scale factors v and $a_{\perp}$. The 'initial' interaction at $s = 0$ is given by the direct interaction: $V(z|s=0) = V_{DI}(z)$

As discussed further below, the RG transformation (5.9) leads to *whole lines of RG fixed points* which describe various types of unbinding transitions. /26,49/ More recently, we have also studied two other functional RG transformations: (i) an *exact* transformation for wetting transitions in $d = 1+1$ with $\tau = 2$ which acts in a somewhat enlarged function space /50/; and (ii) another approximate transformation /51,52/ which is based on a *smooth* cutoff procedure. Apart from the regimes where the unbinding transitions are first-order, the results of these different functional RG methods are in fair agreement.

2. Lines of renormalization group fixed points

Now, let us apply the RG transformation as given by (5.9) within the space of all interactions $V(z)$ which decay to zero for large z at least as $\sim 1/z^{\tau}$. This function space contains both the SFL and the IFL regimes as defined in (5.6) and (5.7). It is convenient to use the dimensionless variables $y \equiv \sqrt{2\zeta} \, z / a_{\perp}$ and $U(y) \equiv 2\zeta \, V(a_{\perp}y/\sqrt{2\zeta}) / v$. Then, the flow equation (5.9) becomes /26/

$$\partial U/\partial s = \zeta[\, \tau U + y \, \partial U/\partial y + ln(1 + \partial^2 U/\partial y^2) \,] \, . \qquad (5.10)$$

The fixed points, $U^*(z)$, of this RG transformation satisfy

$$\tau U^* + y\partial U^*/\partial y + ln[1 + \partial^2 U^*/\partial y^2] = 0 \, . \qquad (5.11)$$

Therefore, the rescaled fixed points depend only on *one* parameter, namely τ. This implies , e.g., that the adhesion of fluid membranes in $d = 3$ is characterized by the same RG fixed points as wetting in $d = 2$ since $\tau = 2$ in both cases. Likewise, (5.10) implies that both systems are characterized, apart from a factor ζ, by the same scaling indices and thus by the same critical exponents.

The fixed point equation (5.11) must be supplemented by appropriate boundary conditions. For unbinding transitions, one wants to include a hard wall at $y = 0$ and a tail which decays to zero for large y. One then finds a line of fixed points, $U^*(y|\sigma)$, parametrized

by a parameter $\sigma > 0$ which behave as /26/

$$U^*(y) = \sigma/y^\tau + \frac{\tau+2}{\tau}\, ln(y) + \mathcal{O}(y^\tau) \quad \text{(with} \quad \sigma > 0) \tag{5.12}$$

for small y and as

$$U^*(y) \approx \rho_L(\sigma)/y^\tau + \rho_S(\sigma)y^{\tau-1} \exp(-y^2/2) \tag{5.13}$$

for large y.

For sufficiently small τ, the function $\rho_L(\sigma)$ is found to be convex downwards with a unique minimum at $\sigma = \sigma_{E1}$. An example is shown in Fig. 6(a) for $\tau = 2$. /26,49/ In this case, the function $\rho_L = \rho_L(\sigma)$ has two zeros at $\sigma = \sigma_{S0}$ and $\sigma = \sigma_{S1}$ (with $\sigma_{S1} < \sigma_{E1} < \sigma_{S0}$) which correspond to short-ranged fixed points with a Gaussian tail, see (5.14). Such a convex downwards piece of $\rho_L(\sigma)$ persists to larger values of τ. However, as τ is increased, the function $\rho_L = \rho_L(\sigma)$ develops more structure. /52/ First, at a certain value $\tau = \tau_2$, it exhibits a point of inflection with zero slope at $\sigma = \sigma_2$ with $\sigma_2 < \sigma_{S1}$ which bifurcates, for $\tau > \tau_2$, into an additional minimum and maximum at $\sigma = \sigma_{E\bar{2}}$ and σ_{E2}. The new minimum at $\sigma = \sigma_{E\bar{2}}$ moves down with increasing τ and touches the σ–axis at $\tau = \tau_{S2} > \tau_2$. An example for the shape of $\rho_L(\sigma)$ with $\tau > \tau_{S2}$ is shown in Fig. 6(b). /52/
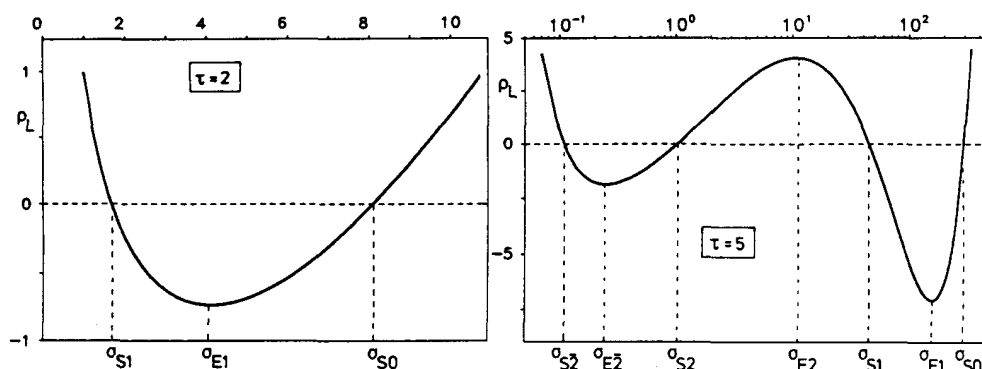
Fig.6: The amplitude $\rho_L = \rho_L(\sigma)$ of the power law tail of the fixed points, see (5.13), for two values of $\tau = d_{||}/\zeta$.

As τ is increased even further, another point of inflection with zero slope appears for $\tau = \tau_3$ which lies at $\sigma = \sigma_3$ with $\sigma_{E\bar{2}} < \sigma_3 < \sigma_{E2}$, i.e., between the minimum and the maximum of the previous bifurcation. /52/ This inflection point develops into another pair of extrema of $\rho_L(\sigma)$ which are located at $\sigma = \sigma_{E\bar{3}}$ and σ_{E3}. This type of bifurcation continues infinitely many times as τ is increased towards $\tau = \infty$: the point of inflection with zero slope for the jth bifurcation at $\tau = \tau_j$ occurs between the two extrema generated in the

(j–1)th bifurcation but it only appears after one of these extrema has touched the σ–axis with $\rho_L = 0$. As a consequence, the function $\rho_L(\sigma)$ exhibits more and more zeroes located at $\sigma = \sigma_{S0}$, σ_{S1} , σ_{S2} and $\sigma_{S\bar{2}}$, σ_{S3} and $\sigma_{S\bar{3}}$ etc. /52,53/ These values of σ are ordered according to $\sigma_{S\bar{2}} < \sigma_{S\bar{3}} < ... < \sigma_{S3} < \sigma_{S2} < \sigma_{S1} < \sigma_{S0}$. They determine the overall shape of the fixed points, $U^*(y)$, as a function of y and , in particular, the number of zeroes of $U^*(y)$ at finite y : for $\sigma \geq \sigma_{S0}$, the fixed points have no extremum and no zero; for $\sigma_{S1} \leq \sigma < \sigma_{S0}$, they have one minimum and one zero; for $\sigma < \min(\sigma_{S\bar{3}}, \sigma_{S2})$ and $\sigma_{S2} \leq \sigma < \sigma_{S1}$, they have one minimum and one maximum and thus two zeros, etc.

3. Relevant scaling fields and scaling indices

The physical meaning of the various fixed points depends primarily on the number and on the character of their relevant perturbations or scaling fields. In the following, I will only consider those perturbations which do not decay more slowly than $1/y^\tau$ (or $1/z^\tau$) for large y (or z), and thus belong to the same subspace of interactions as the fixed points.

For sufficiently large σ, all fixed points are completely stable : all perturbations are irrelevant apart from the marginal one which corresponds to a shift of σ and, thus, to a translation along the line of fixed points. As σ is decreased, a relevant perturbation with eigenvalue $\lambda_1 > 0$ first appears at the location, $\sigma = \sigma_{E1}$, of the minimum of $\rho_L(\sigma)$. This perturbation is in fact short-ranged and has a Gaussian tail as can be shown from the RG transformation (5.10) when linearized around the fixed points. /49/ For $\tau < \tau_2$, no other relevant perturbation is present (within the IFL and SFL regimes) for any value of σ.

For $\tau_2 < \tau < \tau_3$, the function $\rho_L(\sigma)$ has an additional minimum at $\sigma = \sigma_{E\bar{2}}$, and an additional maximum at $\sigma = \sigma_{E2}$, see Fig. 6(b). In the intermediate σ–regime with $\sigma_{E\bar{2}} < \sigma < \sigma_{E2}$, a second relevant perturbation appears with eigenvalue $\lambda_2 > 0$ (which again has a Gaussian tail). As τ is increased beyond τ_3 , the function $\rho_L(\sigma)$ exhibits another maximum and minimum located at $\sigma = \sigma_{E\bar{3}}$ and $\sigma = \sigma_{E3}$, as mentioned. Then, one has three relevant scaling fields for the intermediate σ–range given by $\sigma_{E\bar{3}} < \sigma < \sigma_{E3}$, two relevant scaling fields for $\sigma_{E\bar{2}} < \sigma < \sigma_{E\bar{3}}$ and $\sigma_{E3} < \sigma < \sigma_{E2}$, and one relevant scaling field for $\sigma < \sigma_{E\bar{2}}$ and $\sigma_{E2} < \sigma < \sigma_{E1}$. Thus, each additional inflection point of $\rho_L(\sigma)$ and the associated bifurcation into a maximum and minimum corresponds to the appearance of an additional relevant scaling field (with a Gaussian tail). /52/

4. Critical behavior at unbinding transitions

Within the IFL and the SFL regimes, all fixed points with $\sigma > \sigma_{E1}$ have a domain of attraction with codimension zero, and describe completely *unbound states* of the manifolds. On the other hand, all fixed points with $\sigma < \sigma_{E1}$ have a domain of attraction with a nonzero codimension which is given by the number of their relevant scaling fields. These latter fixed points describe *unbinding transitions* within the IFL and the SFL regimes.

Now, consider a physical system at temperature T with reduced stiffness, K/T, and

reduced direct interaction, $V_{DI}(z)/T$. A change of T now leads to a temperature-trajectory within the interaction space which intersects one of the attraction-domains at the unbinding temperature $T = T_u$. The corresponding fixed point and its relevant scaling fields then govern the critical behavior at T_u. If V_{DI} belongs to the SFL regime defined by (5.7), this fixed point has a Gaussian tail and $\sigma = \sigma_{Sj}$ with $j \geq 1$. If V_{DI} belongs to the IFL regime with $V_{DI}(z) \sim U_{DI}(y) \approx W/y^\tau$, the corresponding fixed point also has such a power law tail with amplitude $\rho_L = W$

In general, $V_{DI}(z)$ may be a complicated function of z and thus may have several minima. Here, I will focus on the situation where $V_{DI}(z) \sim U_{DI}(y)$ achieves a *single minimum* at finite or infinite $z \sim y$. In this case, the critical behavior at the unbinding transitions is governed by the fixed points with $\sigma_{S1} \leq \sigma \leq \sigma_{E1}$

As described above, the function $\rho_L(\sigma)$ has a unique minimum at $\sigma = \sigma_{E1}$ for $\sigma \geq \sigma_{S1}$ Furthermore, the amplitude $\rho_S(\sigma)$ of the Gaussian tail of the fixed points, see (5.13), satisfies $\rho_S(\sigma = \sigma_{S1}) < 0$ and $\rho_S(\sigma = \sigma_{S0}) > 0$. Therefore, for $\sigma_{S1} \leq \sigma \leq \sigma_{S0}$, $\rho_S(\sigma)$ should increase monotonically with σ, and the fixed points can then be parametrized by $\rho_L = \rho_L(\rho_S)$. /49/ This function again has a unique minimum at $\rho_S = \rho_S^*$, and behaves as $\rho_L(\rho_S) \approx \rho_L^* + \frac{1}{2} R_2 (\rho_S - \rho_S^*)^2$ for small $\rho_S - \rho_S^*$. Close to this minimum, the RG flow within the ∞–dim interaction space can be reduced to a flow within the 2-dim (ρ_L, ρ_S) subspace, where it has a parabolic character. /49,4/ Integration of the RG trajectories then leads to two different subregimes, (A) and (B), for the unbinding transitions.

Subregime (A) is governed by the fixed point at (ρ_L^*, ρ_S^*) corresponding to $\sigma = \sigma_{E1}$. A temperature trajectory which intersects the attraction-domain of this fixed point exhibits an unbinding transition of *infinite order* : the mean separation, e.g., behaves as /49/

$$\ell \sim exp[\, 2\pi\zeta \, / \, \omega \, \{\rho_L^* - \rho_L\}^{1/2} \,] \sim exp[\, c \, / \, \sqrt{T_u - T} \,] \quad . \tag{5.14}$$

Subregime (B) is governed by the line of fixed points with $\sigma_{E2} < \sigma < \sigma_{E1}$. In this case, one obtains the power law behavior /49/

$$\ell \sim (T_u - T)^{-\psi} \quad \text{with} \quad \psi \approx \zeta/\omega\{\rho_L^* - \rho_L\}^{1/2} \tag{5.15}$$

as T_u is approached from below. Thus, this regime is characterized by *second-order* transitions but with non-universal critical exponents. It contains the case $\rho_L = 0$ or $\sigma = \sigma_{S1}$ which describes second-order transitions in the SFL regime. In the latter case, the RG considered here leads to a universal value for ψ which depends only on τ. /54/

VI. OUTLOOK

In summary, the shape fluctuations of low-dim manifolds lead to a variety of critical phenomena. As explained in Sec. III, a fluctuating manifold is a scale-invariant object which can be smooth, rough, or crumpled. A rough state consists of humps, a crumpled state of

blobs, see Fig. 1. Furthermore, the manifolds may undergo *roughening, crumpling,* or *unbinding* transitions, as discussed in Sec. III.C and IV, Sec. III.C, and Sec. V, respectively.

Roughening and crumpling transitions can be characterized by the *delocalization* of humps and blobs, see Fig. 2. Such a delocalization also occurs at unbinding transitions where it acts to drive the manifolds apart, see Fig. 5. From a theoretical point of view, the basic scaling properties of these transitions are now understood. As far as experiments are concerned, both roughening /2/ and unbinding transitions /55/ have been observed but more work is highly desirable. In fact, there are many theoretical and experimental problems which deserve further study. Here are just a few of them : (i) *Roughening of quasicrystals* - The results described in Sec. IV imply that the surfaces of *ideal* quasicrystals in d = 3 are always smooth. However, real quasicrystals may contain a certain amount of disorder. It has been argued that interfaces (or domain walls) within *random* quasicrystals are rougher than in periodic structures. /41/ It remains to be shown that this applies also to the *surfaces* of random quasicrystals; (ii) *Crumpling of self-avoiding membranes* - As mentioned, tethered (or polymerized or crystalline) membranes with self-avoidance probably do not crumple. The effect of self-avoidance remains to be understood for more flexible membranes such as fluid or hexatic /25/ ones. One interesting possibility is that the latter membranes undergo a crumpling transition; and (iii) *Adhesion (or unbinding) of vesicles* - Real membranes of amphiphilic molecules usually form closed surfaces or vesicles which often adhere to interfaces or other membranes. We recently found theoretically that such vesicles can also undergo adhesion (or unbinding) transitions. /56/ These transitions should be accessible to various experimental techniques.

Acknowledgements

References

/1/ A review is in R. Lipowsky, in *Random Fluctuations and Growth,* ed. by H.E. Stanley und N. Ostrowsky (Kluwer Academic Publishers, Dordrecht 1988)

/2/ A review is in H. van Beijeren und I. Nolden, in *Structure and Dynamics of Surfaces II,* ed. by W. Schommers und P. von Blanckenhagen (Springer-Verlag, 1987)

/3/ See reviews in *Statistical Mechanics of Membranes and Surfaces,* ed. by D. Nelson, T. Piran, and S. Weinberg (World Scientific, to be published)

/4/ A review is in R. Lipowsky, Physica Scripta T **29,** 259 (1989)

/5/ See, e.g., J.S. Rowlinson und B. Widom, *Molecular Theory of Capillarity,* Clarendon Press, Oxford 1982

/6/ A review is in M.E. Fisher, J. Chem. Soc. Faraday Trans. 2, **82,** 1569 (1986)

/7/   See any textbook on superconductivity.

/8/   See, e.g., *Physics of Amphiphilic Layers,* ed. by J. Meunier, D. Langevin und N. Boccara, Springer Proc. in Physics, Vol. 21 (Springer-Verlag, 1987)

/9/   A review is E. Sackmann, in *Biophysics,* ed. by W. Hoppe, W. Lohmann, H. Markl und H. Ziegler, (Springer-Verlag, 1982)

/10/   W. Helfrich, Z. Naturforsch. **28c,** 693 (1973).

/11/   P.-G. de Gennes und C. Taupin, J. Phys. Chem. **88,** 2294 (1982)

/12/   F.F. Abraham, W.E. Rudge, and M. Plischke, Phys. Rev. Lett. **62,** 1757 (1989), and J.-S. Ho and A. Baumgärtner (to be published)

/13/   P.G. de Gennes, *Scaling Concepts in Polymer Physics,* Cornell University Press, New York 1979

/14/   R. Lipowsky und M.E. Fisher, Phys. Rev. Lett. **56,** 472 (1986),

/15/   C.L. Henley und R. Lipowsky, Phys. Rev. Lett. **59,** 1679 (1987)

/16/   A. Garg und D. Levine, Phys. Rev. Lett. **59,** 1683 (1987)

/17/   G. Grinstein and S.-K. Ma, Phys. Rev. **B 28,** 2588 (1983)

/18/   J. Villain, J. Physique Lett. **43,** L551 (1982)

/19/   D. A. Huse and C. L. Henley, Phys. Rev. Lett. **54,** 2708 (1985)

/20/   T. Nattermann and W. Renz, Phys. Rev. **B 38,** 5184 (1988)

/21/   The unbinding of flux lines has been studied by D. R. Nelson, Phys. Rev. Lett. **60,** 1973 (1988), and K. Ziegler, Europhys. Lett. **9,** 277 (1989)

/22/   T. Nattermann and R. Lipowsky, Phys. Rev. Lett. **61,** 2508 (1988)

/23/   W. Helfrich, Z. Naturforsch. **33a,** 305 (1978)

/24/   R. Lipowsky und S. Leibler, Phys. Rev. Lett **56,** 2541 (1986), and **59,** 1983 (E) (1987)

/25/   D.R. Nelson and L. Peliti, J. Physique **48,** 1085 (1987)

/26/   R. Lipowsky, Europhys. Lett. **7,** 255 (1988)

/27/   S. Leibler and A. Maggs, Phys. Rev. Lett. **63,** 406 (1989)

/28/   Y. Kantor, M. Kardar, and D. R. Nelson, Phys. Rev. **A 35,** 3056 (1987).

/29/   G. Parisi and N. Sourlas, Phys. Rev. Lett. **46,** 871 (1981)

/30/   A. Garg, Phys. Rev. **B 37,** 10003 (1988)

/31/   B. Yang, W. F. Saam, and J. A. Jaszczak (to be published)

/32/   L. Peliti and S. Leibler, Phys. Rev. Lett. **54,** 690 (1985)

/33/   Y. Kantor and D. R. Nelson, Phys. Rev. Lett. **58,** 2774 (1987)

/34/   M. Paczuski, M. Kardar, and D. R. Nelson, Phys. Rev. Lett. **60,** 2638 (1988)

/35/   E. Guitter, F. David, S. Leibler, and L. Peliti, Phys. Rev. Lett. **61,** 2949 (1988)

/36/   R. Lipowsky and A. Baumgärtner, Phys. Rev. **A 40,** 2078 (1989)

/37/   See the collection of reprints in P. J. Steinhardt and S. Ostlund, *The Physics of Quasicrystals* (World Scientific, 1987)

/38/   C. Tang and M. Kohmoto, Phys. Rev. **B 34,** 2041 (1986)

/39/   M. Kohmoto, B. Sutherland, and C. Tang, Phys. Rev. **B 35,** 1020 (1987)

/40/   S. Aubry and G. Andre, in *Group Theoretical Methods in Physics,* ed. by L. Horwitz and Y. Ne'eman, Annals of the Israel Phys. Soc., Vol. 3, and Ref. /37/

/41/   R. Lipowsky and C. L. Henley, Phys. Rev. Lett. **60,** 2394 (1988)

/42/   D. A. Huse, (unpublished)

/43/   Similar results have been obtained by L. V. Mikheev, Phys. Lett. **A 132,** 137 (1988)

/44/   J. A. Jaszczak, W. F. Saam, and B. Yang, Phys. Rev. **B 39** (in press)

/45/   See, e.g., R. Lipowsky, Phys. Rev. **B 32,** 1731 (1985), and *Critical behavior of interfaces: wetting, surface melting and related phenomena,* Habilitations-Schrift, Universität München, 1987 (published as Juel-Spez-438 by KFA Jülich)

/46/   R. Lipowsky und M.E. Fisher, Phys. Rev. **B36,** 2126 (1987)

/47/   R. Lipowsky und M.E. Fisher, Phys. Rev. Lett. **57,** 2411 (1986)

/48/   K.G. Wilson, Phys. Rev. **B4,** 3184 (1971); K.G. Wilson and M.E. Fisher, Phys. Rev. Lett. **28,** 240 (1972)

/49/   R. Lipowsky, Phys. Rev. Lett. **62,** 704 (1989)

/50/   F. Jülicher, R. Lipowsky, and H. Müller-Krumbhaar, (to be published)

/51/   S. Scheidl, diploma thesis, Universität München, 1989

/52/   S. Grotehans and R. Lipowsky, (to be published)

/53/   The fixed points with $\rho_L = 0$ have been independently studied by F. David and S. Leibler, (to be published)

/54/   This is consistent with the MC data on the adhesion transitions of fluid membranes as obtained by R. Lipowsky and B. Zielinska, Phys. Rev. Lett. **62,** 1572 (1989)

/55/   Adhesion transitions of fluid membranes have been experimentally observed by M. Mutz and W. Helfrich, Phys. Rev. Lett. **62,** 2881 (1989)

/56/   U. Seifert and R. Lipowsky (to be published)